Article:
Zhao, J, Yao, G, Ramisetti, SB orcid.org/0000-0002-2927-5257 et al. (2 more authors) (2018) Molecular Dynamics Simulation of the Salinity Effect on the n-Decane/Water/Vapor Interfacial Equilibrium. Energy and Fuels, 32 (11). pp. 11080-11092. ISSN 0887-0624

https://doi.org/10.1021/acs.energyfuels.8b00706

Molecular Dynamics Simulation of the Salinity Effect on the n-Decane/Water/Vapour Interfacial Equilibrium

Jin Zhao[1], Guice Yao[1], Srinivasa B. Ramisetti[1], Robert B. Hammond[1], Dongsheng Wen[2, 1*]

[1]School of Chemical and Process Engineering, University of Leeds, Leeds, LS2 9JT, UK

[2]School of Aeronautic Science and Engineering, Beihang University, Beijing, 100191, P. R. China

Abstract: Low-salinity water flooding of formation water in rock cores is, potentially, a promising technique for enhanced oil recovery (EOR), but details of the underlying mechanism remain unclear. The salinity effect on the interface between water and oil was investigated here using the Molecular Dynamics (MD) simulation method. n-Decane was selected as a representative oil component, SPC/E water and OPLS-AA force fields were used to describe the water/oil/ionic interactions for salt water and n-decane molecules. Equilibrium MD simulations were firstly conducted to study the n-decane/vapour and salt-water/vapour interface systems at six different NaCl concentrations (0 M, 0.05 M, 0.10 M, 0.20 M, 0.50 M and 1.00 M). The water/oil interface was then investigated by calculating bulk density distribution, radial distribution function, interface thickness and water/oil interfacial tension (IFT). Sufficiently long MD simulations of water/n-decane/vapour were performed, followed by an analysis of the effect of salinity on the water/oil/vapour interface. The IFT values for the water/vacuum interface, n-decane/vacuum interface and water/n-decane interface were obtained from the pressure tensor distribution after system equilibration, with values of 71.4, 20.5 and 65.3 mN/m, respectively, which agree well with experimental and numerical results reported in the literature. An optimal salinity of ~0.20 M was identified corresponding to a maximum interfacial thickness between water and oil phase, which results in a minimum water/oil IFT value and a maximum value for the oil/water contact angle, a condition beneficial for enhanced oil recovery.

KEY WORDS: Low salinity flooding, Molecular Dynamics Simulation, Interfacial Tension, Wettability, Enhanced Oil Recovery

1. INTRODUCTION

Enhanced oil recovery (EOR) is becoming more and more important to maximize recovery from existing oil fields to meet the increasing global energy demand and to mitigate environmental impact [1]. Low salinity flooding, i.e. injecting lower-salinity water (usually specified as having a 1:1 electrolyte concentration of less than about 5,000 ppm) into formation water, has been of interest as an EOR technique [2] since the publication of the first experimental evidence by Jadhunandan and Morrow [3]. It was soon found that an enhancement is not observed consistently but is dependent on a number of factors, including connate water saturation, the salinity of connate water, injection water salinity, and wettability [4]. No less than seventeen recovery mechanisms behind the low-salinity EOR process have been proposed in the literature, but many of them are related to one another [5]. Due to the complexities of oil components and reservoir rock formations, the recovery mechanisms underpinning the low-salinity EOR process are still unclear. Two physical properties which, when manipulated, are influential on low-salinity EOR phenomena are substrate wettability and the interfacial tension (IFT) between the oil and brine (when reduced) [6]. The interfaces between immiscible liquids are therefore fundamental in understanding EOR mechanisms. Interfaces are, by definition, discontinuities in nature but it must also be recognised that there is a fundamental difference between a single interface considered in isolation, e.g. between two immiscible liquid components in the bulk, and two or more interfaces in very close proximity for example having two solid-surfaces separated by a thin liquid-layer comprised of two immiscible liquid-components such as aqueous electrolyte and a hydrocarbon.

The interfacial tension (IFT) between oil and water is one of the key properties determining the mobility of trapped oil in reservoir rocks [7-10]. Experimentally the effect of salts on IFT and consequently on oil recovery efficiency has been investigated for several decades, but with contradictory results. For instance, Aveyard et al. [11] first reported that the IFT increased linearly for the dodecane-water system as the molality of electrolyte of different kinds is increased except in the case of potassium iodide, which showed a decreasing trend. Later, Ikeda et al. [12] measured the IFT of water/hexane as a function of sodium chloride concentration using the pendant drop method and showed an increase of IFT when increasing the salt concentration from 0 to 1 molar, which is consistent with results from Badakshan et al. [13] and Cai et al. [14]. In contrast, Serrano et al. [15] observed fluctuations in IFT values for oil/brine at different salt concentrations, and Alotaibi et al. [16] indicated that low salinity did not always reduce the IFT of water/n-dodecane. After reaching equilibrium at five minutes of elapsed time, the IFT of the 5 wt% NaCl solution decreased in contrast with two other concentrations 2 and 10 wt% respectively [16]. The exact causes of such contradictory observations regarding the effect of salts on IFT remain unclear and require fundamental insights at the molecular level. To this end, a few experimental studies at the molecular scale have been carried out at liquid/solid interfaces, e.g., by X-ray crystallography, to understand the properties of water molecules located next to hydrophobic surfaces, including the orientation of water molecules and their hydrogen bonding interactions [17, 18]. However, experimental measurements for liquid-liquid interfaces at nanoscale are still very difficult to achieve because such interfaces are diffuse in comparison with solid/liquid interfaces. Consequently, experimental measurements at liquid/liquid interfaces are often associated with large uncertainties, and the detection of the influence of structural properties of oil at the interface is challenging.

Whereas a suitable continuum model may be sufficient to model the interface between water and oil components in the bulk, and its sensitivity to the aqueous electrolyte concentration, an atomistic modelling approach can yield significant insights into the effect of a reduction in the smallest length-scale which defines the separation distance between two solid surfaces when modelling a pore in an oil-reservoir rock. An appropriate atomistic approach to explore effects associated with confinement and small length-scales is classical Molecular Dynamics (MD), which has been recently adopted to provide fundamental information on the molecular interactions and fluid flow at nanoscale. A few MD studies have been conducted for EOR applications [19, 20], including the prediction of thermo-physical properties such as viscosity and thermal conductivity [21-23]. On the interfacial properties, Jungwirth et al. [24] investigated the effect of inorganic ions on the air/water interface by MD simulation, and found that the simulation results were consistent with experimental evidence. D'Auria et al [25, 26] carried out both dissipative particle dynamics (DPD) and classical MD simulations of aqueous solutions of sodium chloride at two different concentrations using polarizable and standard additive force fields, showing that the presence of chloride ions at the air-solution interface is reconcilable with the classical thermodynamics results of Gibbs absorption theory. Sun et al. [27] investigated surface tension and structure of salt solutions and clusters and showed that the van der Waals interactions had a large impact on the distribution of the halide anions and that conventional force field parameters needed to be optimized to increase the accuracy of IFT prediction. Buuren et al. [28] performed MD simulations on the sensitivity of surface properties to the van der Waals parameters for the decane/ water interface, followed by Zeppieri, Jang, and Mitrinovic et al. [29-31]. Kunieda et al. [32, 33] investigated the spreading of multi-component oils on water with MD simulations, and predicted the IFTs between water and oil-mixture components including decane, toluene and heptane. Zhang et al. [34] investigated the structural and dynamical properties of the NaCl solution/n-decane interface, and found that

NaCl salts did cause an increase in the surface tension but did not affect the molecular orientation significantly. These studies showed that properly used, MD could provide fundamental information, inaccessible via experimental measurements, into the structure properties of interfacial systems. The current MD studies, however, have been exclusively focused on two-phase equilibrium between water and a single oil component, the presence of substrate and the vapour phase, which could have significant influence on the interfacial properties, has not been considered explicitly.

Four interface systems were investigated by MD simulations in this paper, namely n-decane/vapour interface, water/vapour interface, salt-water/n-decane interface, and salt-water/decane/vapour interface systems, respectively. The purpose of this contribution is twofold, firstly to demonstrate the suitability of the choice of interatomic force field and calculation set-up by applying MD to model the bulk interface between vapour and liquid phases (water, containing varying concentrations of sodium chloride, and n-decane); and secondly to apply the approach to the more complex cases of the salt water/n-decane interface and salt water/n-decane/vapour interface systems. The influences of aqueous NaCl solutions at six different concentrations from, 0.00 M (deionized water) to 1.00 M, were examined to investigate salinity effects at the interface. The species' radial distribution function (RDF), density distributions, interface thickness, contact angle and the IFT were calculated and analysed in each system to reveal the fundamental influence of salts for low-salinity EOR application.

2. METHODOLOGY

The details about model construction are presented in this section. The MD simulation technique is described along with details of how the molecular pressure tensors, density

profiles, interfacial tension and interfacial thickness were extracted from the simulation trajectory files.

2.1 Model Construction

To investigate the salinity effect on the water/oil/vapour interfacial equilibrium, n-decane ($C_{10}H_{22}$) molecules were considered as representative of the oil phase, decane being a typical component of petroleum, and one presented frequently in the literature as a kerosene surrogate, or as the main component of diesel surrogates. Aqueous NaCl solutions were selected as a representative 1:1 electrolyte with six different salt concentrations, which were 0.00 M (deionized (DI) water), 0.05 M, 0.10 M, 0.20 M, 0.50 M, and 1.00 M, respectively.

Figure 1 shows the simulation procedure and the initial configurations of systems: (a) the validation of our simulations is firstly demonstrated by a careful benchmark of the approach on smaller systems representing n-decane/vapour and salt-water/vapour interfaces. In Section 3.1: both the n-decane/vapour interface system and salt-water/vapour system were constructed by building one n-decane or water slab in the middle of a cubic box with two vapour spaces either side; (b) to investigate the salt-water/n-decane interface in Section 3.2, two rectangular aqueous electrolyte blocks were built, separated by a distance of 4.0 Å, and the intervening volume element was filled with randomly orientated n-decane molecules; (c) for the salt-water/n-decane/vapour interface system reported in Section 3.3, a three-phase system was established to visualise the contact angle directly by initially inserting an n-decane droplet onto a water slab, with a separation distance of 4.0 Å. It is notable that this salt-water/n-decane/vapour three-phase system was made as an apparent two-dimensional system. The advantages of such an approach compared with a fully 3D model are as follows: i) computational time can be saved since a small length in the depth direction can be taken; ii) effects caused by droplet size on the contact angle can be ignored, since the radius of curvature

is infinity on the straight three-phase contact line. The Packmol [35] package was used to construct all the initial configurations for the simulations with both water and n-decane molecules randomly distributed and orientated in the simulation box initially.

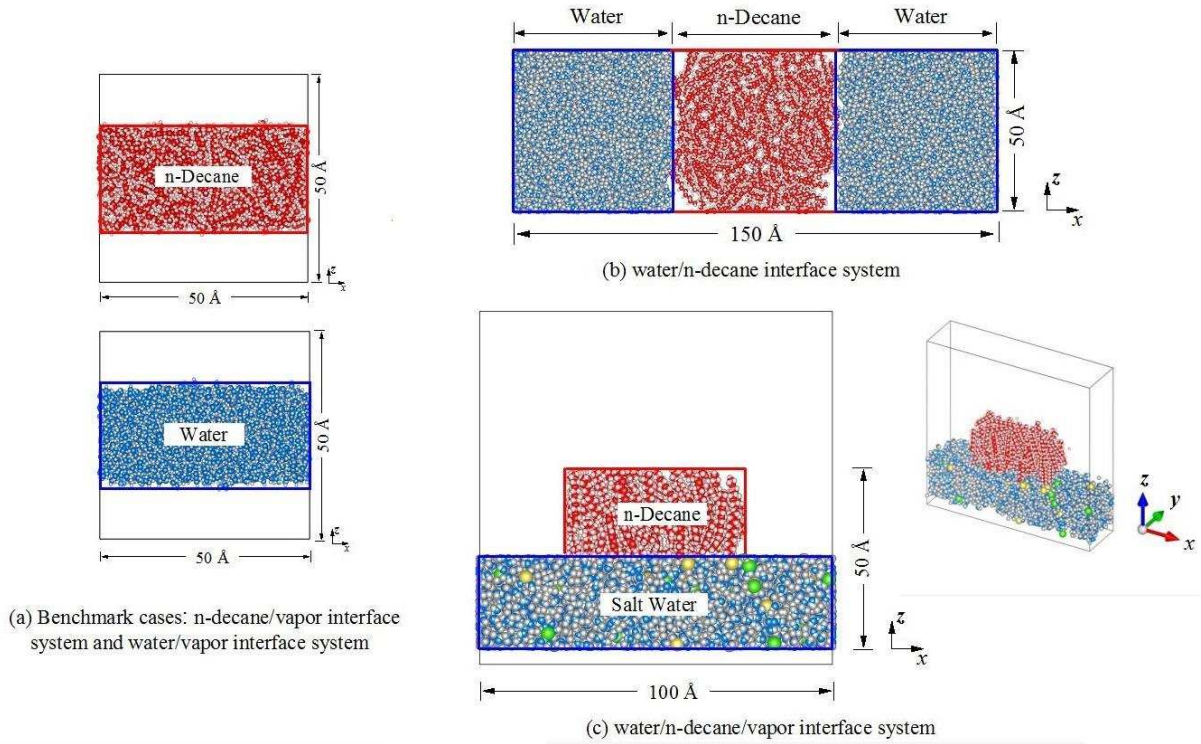

Figure 1 Initial configurations of the simulated systems

To remove any high strain for the initial configurations, energy minimization was performed using the steepest descent method before the equilibrium MD simulations were carried out. Periodical boundary conditions were used in all systems with different spatial dimensions as shown in Figure 1(a-c) with a total density of 1.00 g/cm^3 for the water phase and 0.73 g/cm^3 for the oil phase.

2.2 Force Fields

In these simulations, n-decane interactions were described using the all-atom model of the OPLS-AA force field [21], and the SPC/E force field was used for water [22]. The sodium

and chloride ions were modelled as charged Lennard-Jones particles [36] by also using parameterizations of the OPLS-AA force field. These force fields were tested extensively and successfully used in previous simulations [8, 37-39]. The total energy is given by Equation 1, including both the intra- and intermolecular interactions:

$$E_{total} = E_{bond} + E_{angle} + E_{dihedral} + E_{torsion} + E_{vdw} + E_{coulombic} \quad (1)$$

where E_{total}, E_{bond}, E_{angle}, $E_{dihedral}$, $E_{torsion}$, E_{vdw} and $E_{coulombic}$ are the total energy, bond-stretching, angle-bending, dihedral-energy, torsion energy, van der Waals and electrostatic components, respectively. The Lennard-Jones potential parameters (ε_{ij} and σ_{ij}) between different atom types, were obtained using geometric combining rules as shown in Equations 2 and 3:

$$\sigma_{ij} = \sqrt{\sigma_{ii}\sigma_{jj}} \quad (2)$$

$$\varepsilon_{ij} = \sqrt{\varepsilon_{ii}\varepsilon_{jj}} \quad (3)$$

In the simulations, all the atoms were free to adjust their positions to attain equilibrium structures.

2.3 Equilibrium molecular dynamics simulation details

All equilibrium MD calculations were performed using the DL_POLY molecular simulation package [40]. The Leapfrog integration algorithm was used with a time step of 1.0 fs in all simulations. The potential energy was evaluated with a 10.0 Å cut-off distance for the short-range van der Waals interaction, and a comparison with further simulations using a larger cut-off distance of 12.0 Å was conducted to check that the simulations employing a 10.0 Å cut-off were energy converged. The Ewald summation for the Columbic interactions (Smoothed Particle Mesh Ewald in DL_POLY) was calculated with a precision of 1×10^{-6}. A Berendsen thermostat with a relaxation time of 0.1 ps was used to control the system temperature. To

remove initial strain, energy minimization (steepest descent) was performed on the initial configuration for 1×10^4 steps. The MD simulation was subsequently started in the NPT ensemble with an equilibration period of 50 ps at 0.10 MPa and with initial velocities taken for a Maxwellian distribution at 300 K and meanwhile coupling the system to an external heat bath at 300 K with a constant time step of 0.001 ps. After equilibration, the volume of the system was then kept fixed, and another 5 ns of NVT ensemble simulation was conducted with all covalent bond lengths, as well as the water bond angle, constrained by the procedure SHAKE (tolerance 1×10^{-5} nm).

2.4 Calculation Methods

Here, the pressure tensor for the interface system was obtained by using the virial equation, Equation 4,

$$P_{\alpha\beta} = \frac{1}{V}\left(\sum_{i=1}^{N} m_i v_{i\alpha} v_{i\beta} + \sum_{i=1}^{N-1}\sum_{j=i+1}^{N} F_{ij\alpha} r_{ij\beta}\right) \quad (4)$$

where, $P_{\alpha\beta}$ is an element in the pressure tensor, α and β are the directional components; V is the volume, m_i is the mass of particle i, $v_{i\alpha}$ is its velocity in the α direction, $F_{ij\alpha}$ is the α component of the total force on particle i due to particle j, and $r_{ij\beta}$ is the β component of the vector (r_i - r_j). The kinetic contribution to the pressure is given by the first term in this equation, and the virial contribution is given by the second. The three diagonal elements in the pressure tensor represent the relevant pressure components.

The interfacial tension γ of the salt-water/n-decane interface normal to the z-axis can be calculated from the pressure tensor distribution after equilibration using the mechanical definition [41, 42] as Equation 5

$$\gamma = -\int (p'(z) - p)dz \quad (5)$$

where p′(z) is the lateral pressure, p is the bulk pressure, and the integral is defined over the boundary layer. With two interfaces perpendicular to the z axis, this gives the following relationship, Equation 6, for the interfacial tension

$$\gamma = -\frac{1}{2}\left(\frac{p_x+p_y}{2} - p_z\right)L_z \quad (6)$$

in which $p_\alpha = P_{\alpha\alpha}$ (α = x, y, z) and L_z is the box length in the z direction used for the calculation. For the three-phase water/n-decane/vapour systems, by assuming that the local interfaces far from the three phase contact line are parallel to xy-plane, the local pressure distributions were used over the range of 40 ≤ x ≤ 60 Å and 20 ≤ x ≤ 60 Å when calculating the water/decane interfacial tension, which can be expressed as:

$$\gamma = -\left(\frac{p_x+p_y}{2} - p_z\right)L_z \quad (7)$$

The planar density profiles for the simulations can be used to describe the probability of finding an atom within a planar element df_c along a Cartesian axis, using Equation 8

$$\rho(f_c) = n_f / N df_c \, . \quad (8)$$

where the value N is the number of total atoms and n_f is the number of atoms within a planar element df_c.

To characterize the thickness of the vapour/liquid interface in the simulations, the "10–90" interfacial thicknesses, t, are obtained by fitting each of the two equilibrium molecular density profiles, ρ(z), to a hyperbolic tangent function of the form given in Equation 9 [43],

$$\rho(z) = \frac{1}{2}(\rho_L + \rho_V) - \frac{1}{2}(\rho_L - \rho_V)\tanh\left(\frac{z-z_0}{t}\right) \quad (9)$$

where ρ_L and ρ_V are the liquid and vapour densities, respectively, z_0 is the location of the Gibbs dividing surface, and the interface thickness t is calculated as the distance between two positions where the density varies from 10% to 90% of the density of the bulk phase. As a

result, this thickness is known as the "10-90" interfacial thickness. A frequently used alternative thickness is the "10-50" interfacial thickness which is defined analogously. To be more specific, the "10-90" interfacial thickness criterion was adopted by defining the interfacial thickness to be the distance along the interface over which the density changes from a value of 10% to 90% of the total density change between the bulk, i.e., the spatial extent over which the density varies from $\rho_{VB}+0.1(\rho_{LB}-\rho_{VB})$ to $\rho_{VB}+0.9(\rho_{LB}-\rho_{VB})$, where ρ_{VB} *and* ρ_{LB} are the vapour and liquid bulk densities, respectively.

For systems exhibiting liquid-liquid equilibrium, the thickness of the water/n-decane interface was calculated using the criteria proposed by Senapati and Berkowitz [44]. The density profile of each component is fitted to an error function form given by Equations 10 and 11,

$$\rho_W(z) = \frac{1}{2}\rho_{WB} - \frac{1}{2}\rho_{WB}\mathrm{erf}\left[\frac{z-\langle z_W\rangle}{\sqrt{2}t_C}\right] \tag{10}$$

$$\rho_D(z) = \frac{1}{2}\rho_{DB} + \frac{1}{2}\rho_{DB}\mathrm{erf}\left[\frac{z-\langle z_D\rangle}{\sqrt{2}t_C}\right] \tag{11}$$

where $\rho_W(z)$ and $\rho_D(z)$ are the density profiles of water and decane, respectively; ρ_{WB} *and* ρ_{DB} are the water and decane bulk densities, respectively; $\langle z_W\rangle$ and $\langle z_D\rangle$ are the average positions of the individual Gibbs dividing surfaces for each interface; and erf is the error function. The contribution from the intrinsic width to the interfacial thickness t_0 is determined from the difference between the positions of the fitted interfaces as $t_0=|\langle z_D\rangle-\langle z_W\rangle|$; the contribution of thermal fluctuations to the interfacial width is determined by the value of the "10–50" interfacial thickness t_C. The total interfacial width is then given by Equation 12,

$$t^2 = t_0^2 + t_C^2 \tag{12}$$

3. RESULTS AND DISCUSSION

Section 3.1 discusses the validity of the choice of interatomic force field and calculation set-up through applying MD to model two validation cases (n-decane/vapour and salt-water/vapour interfacial equilibrium systems). Sections 3.2 and 3.3 report the salinity effect on the salt-water/decane interface and salt-water/decane/vapour interface at six electrolyte concentrations.

3.1 Benchmark cases for validation: (a) n-decane/vapour interfacial equilibrium and (b) effects of salinity on the salt-water/vapour interfacial equilibrium simulations

The validation of our simulations is demonstrated by a careful benchmarking of the approach on simpler systems namely n-decane/vapour and salt-water/vapour interfaces as reported in this section. After 5 ns of simulation time for both systems, the energy, pressures and temperatures of all components were considered to be equilibrated. This was checked in one case by extending the simulation time by a further 3 ns with no significant changes observed in the relevant parameter values. It should be noted that the calculated densities of the n-decane phase in the n-decane/vapour system (0.728 ± 0.063) and water phase in each salt-water/vapour systems (0.998 ± 0.027) agree well with those of the pure bulk phases (0.73 g/cm^3 for n-decane and 1.00 g/cm^3 for water). This shows that the simulations are sufficiently long for studying a realistic interface between two bulk phases.

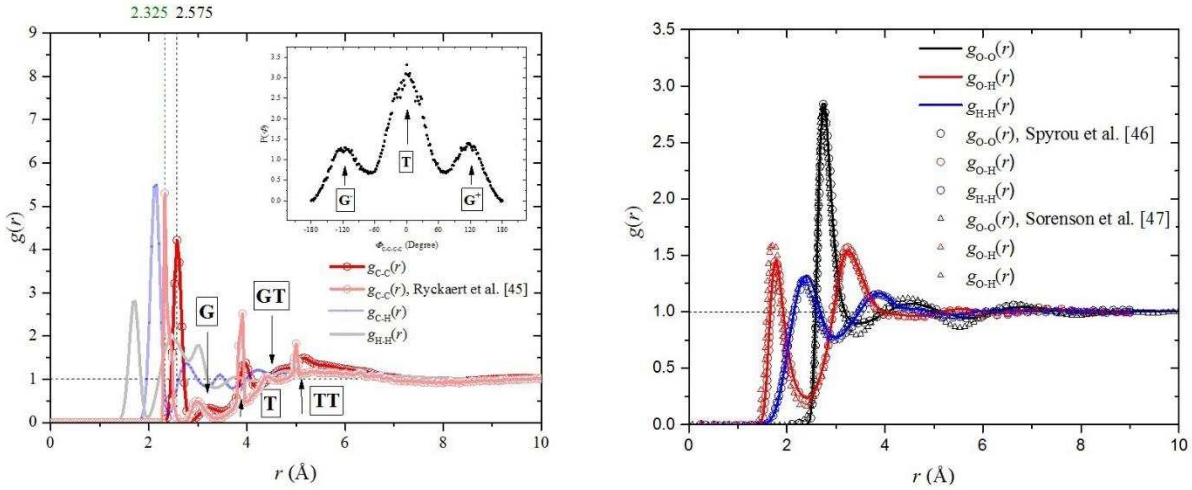

(a) RDFs for the n-decane/vapour interface system (b) RDFs for the DI-water/vapour interface system

Figure 2 Radial distribution function (RDF) profiles for the n-decane/vapour interface and DI-water/vapour interface systems [45-47]

The radial distribution function (RDF) of molecules in both n-decane/vapour and DI-water/vapour interface systems were sampled as shown in Figure 2: (1) The interaction between two n-decane molecules can be seen from the RDF profiles in Figure 2(a), where intra- and inter-molecular correlations are mixed. As far as the intermolecular correlations are concerned, it is clear that the oscillations around g(r) = 1 are close to the cutoff radius. Trans (T) and Gauche (G) conformation positions of carbon atom neighbours in a molecule can also be observed, followed with successive GT and TT conformations as marked in Figure 2(a). To characterize the conformations of n-decane molecules in the n-decane/vapour interface system, the probability density functions (PDF) distribution for the n-decane molecules as a function of the internal dihedral angle $\Phi_{C\text{-}C\text{-}C\text{-}C}$ was calculated as shown in Figure 2(a), where the peaks observed at $\Phi_{C\text{-}C\text{-}C\text{-}C} = 0°$ and $\Phi_{C\text{-}C\text{-}C\text{-}C} = \pm 120°$ correspond respectively to trans (T) and gauche (G^+ and G^-) conformations. The magnitudes of the G^+ and G^- peaks are very close, corresponding with the symmetry of the dihedral potential energy. (2) The RDFs between water molecules are presented in Figure 2(b). It can be observed that g(r) equals 0 at short distance, which indicates strong repulsive forces between two water molecules in the short range. The

first peak occurs at 2.8 Å with g(r) arriving around a value of 3, which can be interpreted as indicating that it is three times more likely to find two oxygen atoms in different water molecules at this separation. At longer distances, g(r) between two water molecules approaches a value of one indicating there is no long-range order. The RDF profiles of both n-decane and water components are in good agreement with previous MD simulations and experimental results with no shifts for the two main peaks [45-47].

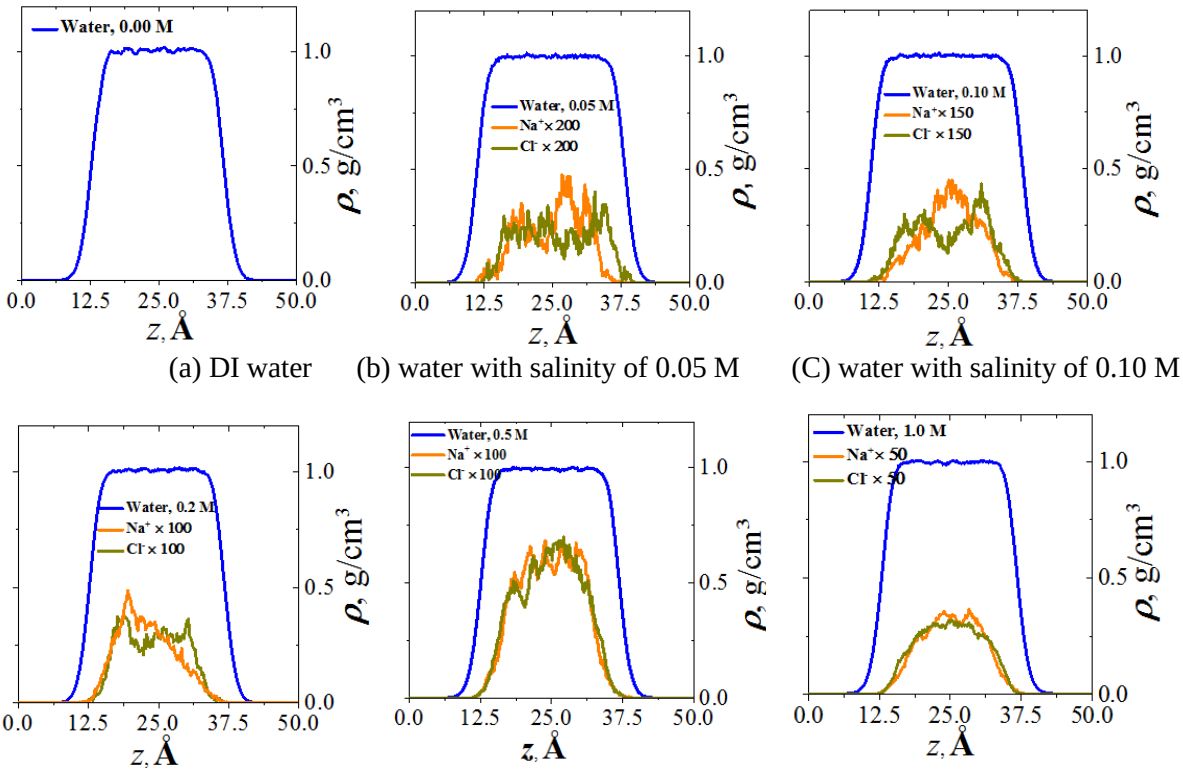

(a) DI water (b) water with salinity of 0.05 M (C) water with salinity of 0.10 M

(d) water with salinity of 0.20 M (e) water with salinity of 0.50 M (f) water with salinity of 1.00 M

Figure 3 Z-density profiles for the various components of the six aqueous NaCl solution systems

A series of 5 ns MD simulations of aqueous NaCl solutions at different concentrations (0.00 M, 0.05 M, 0.10 M, 0.20 M, 0.50 M and 1.00 M) were also performed for investigating the salinity effect on the water/vapour interface. The structure of the salt-water/vapour interface was investigated by calculating the mass density profiles along z direction perpendicular to the interfacial plane xy, as shown in Figure 3. The results show that the ion concentration has little

effect on the bulk water density, with a stable overall value around 1.0 g/cm^3. Besides, although ions move thermodynamically within the water phase as shown in Figure 6, both sodium and chloride ions are repelled from the water/vapour interface, leaving an almost ion-free interface layer, as shown in the ion density distribution profiles in Figure 3. This phenomenon behaves in accord with the standard theory of the air/water interface for electrolytes [48] and is reflected experimentally by an increase in the measured surface tension. When the water salinity is lower than 0.20 M, the chloride ions penetrate towards the interface next to the ion-free layer, and exhibit a concentration peak, followed by a subsurface depletion. The repulsion of counter-ions and the subsurface neutrality requirement demonstrates the fact that the sodium cations are dragged by the anions and consequently exhibit a subsurface peak. However, this effect becomes weakened when the water salinity is larger than 0.20 M.

To further confirm that an equilibrated system had been obtained in the simulations, the IFT between salt water and the vapour phase was calculated from the molecular pressure tensor with 1 ns of time averaging, as displayed in Figure 4. The "block averaging" approach, firstly reported by Flyvbjerg and Petersen [49], was adopted in this work to determine the property value for a give variable, which has been identified as a simple, relatively robust procedure for estimating statistical uncertainty [50]. The standard error for the interfacial tension was calculated from 10 interfacial tension values by using the pressure tensor, for which each value was obtained from a 0.2 ns length of the local pressure distribution data following equilibration. The typical equilibrated n-decane/vapour and DI-water/vapour IFT values of 20.54 ± 1.87 mN/m and 71.43±0.57 mN/m are obtained by averaging the last 2 ns of the trajectory with an averaging step of 10 ps. In previous MD simulations, even here conflicting water/vapour IFT values are reported despite the use of the same SPC/E potential in the simulations, values varying from 55.4 to 72 mN/m, as summarized in Table 1 below.

Table 1. SPC/E-water/vapour IFT from different MD simulations (Unit: mN/m)

	Our result	Neyt et al. [51]	Underwood et al. [36]	Vega et al. [52]	Chen et al. [53]	Shi et al. [54]	Lv et al. [55]	Ismail et al. [56]	Alejandre et al. [57]
SPC/E	71.43	62.4	61.8	63.6	65.3	72.0	70.1	55.4	71.5

The conflicting values of surface tension for the SPC/E water system can mostly be traced to a variety of numerical issues, resulting from the use of: different size-dependent systems, different ensembles (NPT or NVT), different thermostats (Nooser-Hoover or Berendsen), combining different methodologies for determining the electrostatic interactions (e.g., PPPM and PME), or using alternatively the SHAKE or SETTLE algorithm to constrain the water molecule geometry, etc.. Our calculated value of 71.43 mN/m using the SPC/E water model at 300 K appears to be in good agreement with three studies of the surface tension of SPC/E water Alejandre et al. [57], Shi et al. [54], Lv et al. [55], and Jungwirth et al. [58] respectively, and also compares well to the experimental value of 71.3~71.6 mN/m, indicating the validity and stability of our calculation setup.

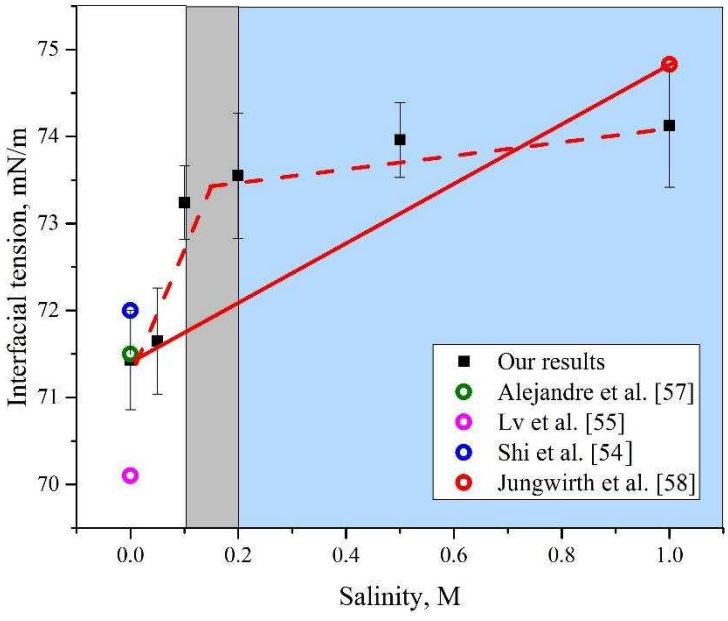

Figure 4 The salinity effect on the interfacial tension of the water/vacuum interface

In agreement with experimental measurements, results from the MD simulations shown in Figure 4 indicate that, (a) the interfacial tension of the NaCl solutions is greater than that of

pure water, and (b) increasing the NaCl concentration increases the surface tension of the solution/vapour interface. It may be noted that when computing the surface tension from the pressure tensor distribution the increase in salt-water/vapour IFT appears not to be a linear function of the water salinity : Starting from a salinity around 0.10 ~ 0.20 M, the rate of increase in the simulated IFT becomes less (though continuously increasing, there is an "inflection point" of IFT at the salt concentration ~ 0.20M.). This phenomenon has been mostly neglected in previous experiments /simulations by simply concluding that surface tensions of inorganic electrolyte aqueous solutions were often summarized to be linear functions of salt concentration. However, these simple linear relationships may not be sufficient to explain observations at the nano-scale, where deviations of water/vapour IFT from the monotonic linear increase exist, e.g., (i) the MD results from Bhatt et al. [59]; (ii) MD results also using SPC/E water model by Wang et al. [60], and (iii) those determined by the DKA approach [61]. Using the same MD simulation method and calculation setup, the interface systems between salt water and the n-decane phase were simulated and the results are reported in the next section.

3.2 Effects of salinity on salt-water/n-Decane Interfacial Equilibrium

The salinity effect on the water/n-decane interface system is reported in this section at six electrolyte concentrations of 0.00 M, 0.05 M, 0.10 M, 0.20 M, 0.50 M and 1.00 M, respectively.

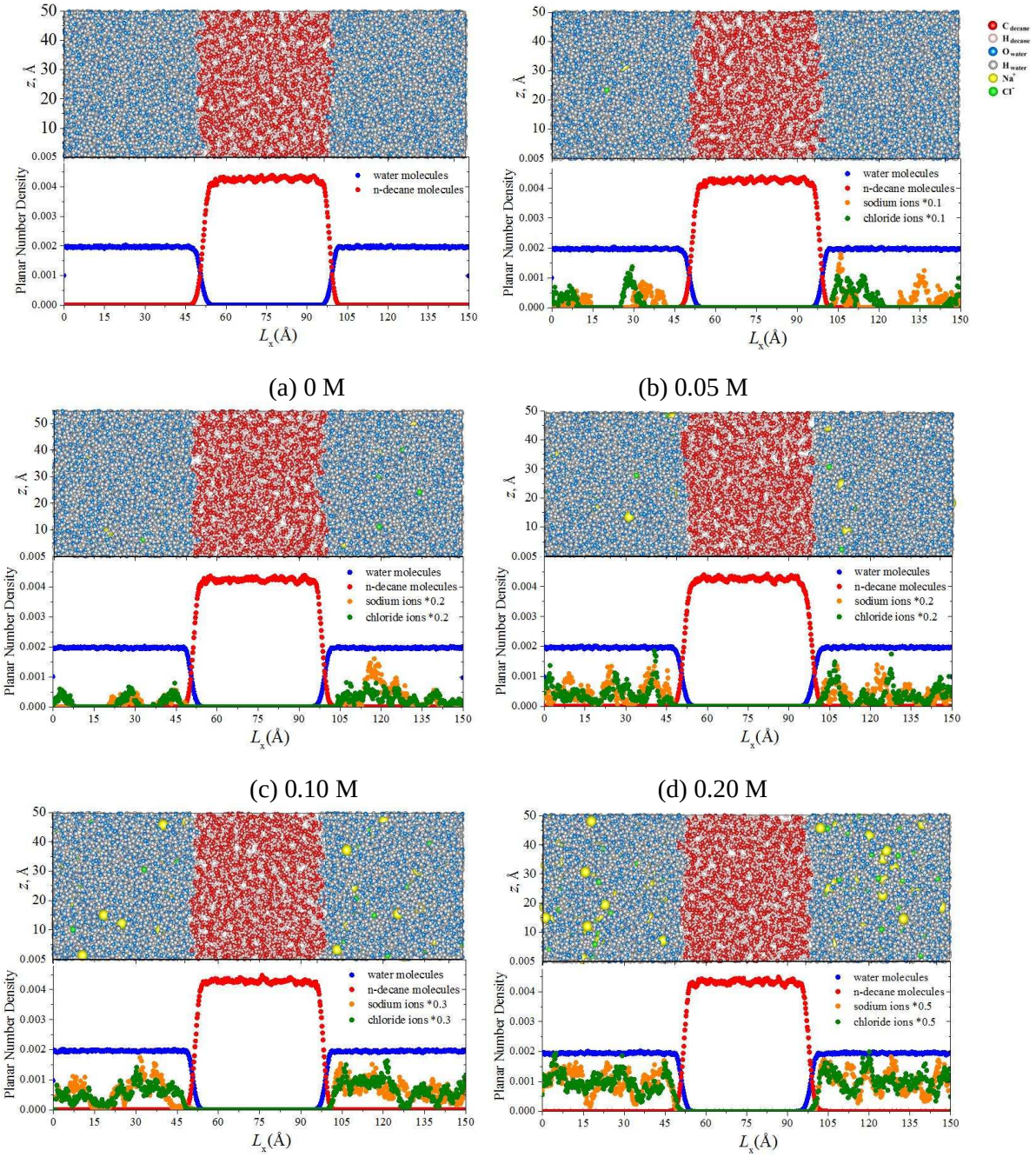

(a) 0 M (b) 0.05 M

(c) 0.10 M (d) 0.20 M

(e) 0.50 M (f) 1.00 M

Figure 5 n-decane/salt-water equilibrated interfaces at different salinities

Figure 5 presents the final equilibrium-configuration snapshots of the salt-water/n-decane interface system after 5 ns simulations representing different NaCl concentrations, along with the number density profiles of each system along the x-axis direction, perpendicular to the water/n-decane interface. It is clear that in every case the salt-water/n-decane system

consists of two phases with two, well-defined interfaces, as can be deduced from the representation of the water and organic phase molecular density along the direction perpendicular to the interface, representing the immiscibility of salt water and organic phases. In addition, an almost ion-free layer can also be observed at the salt water/n-decane interface.

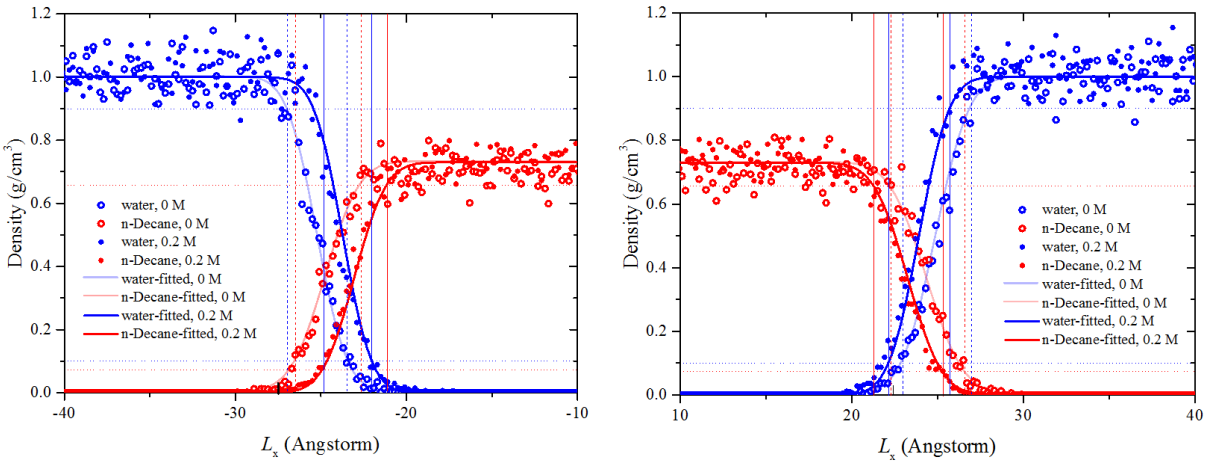

Figure 6 Planar (yz) density profiles $\rho(f_c)$ as a function of the box length L_x system and the definition of "10-50" interfacial thickness for the salt water/n-decane system

To characterize the salt water/n-decane interface thickness, the "10-50" interfacial thickness criterion, derived from the density profiles, of both salt water and n-decane phases along the x-axis direction in the salt water/n-decane interface system are illustrated in Figure 6 for salt concentration of 0.00 M and 0.20 M. Bulk density values for the water and n-decane phases are observed with values around 1.00 and 0.73 g/cm^3, respectively, with the interface density transition profiles in between.

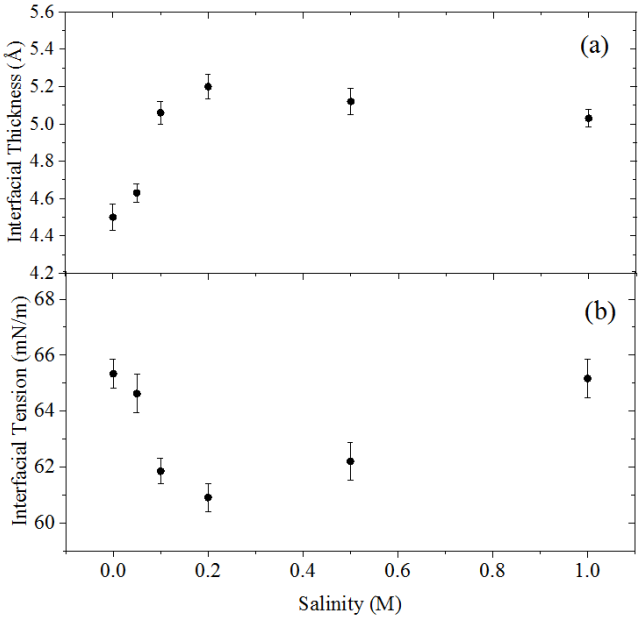

Figure 7 (a) "10-50" interfacial thickness, and (b) interfacial tension as function of salinity for n-decane/salt water interface

Table 2 Interfacial thickness and IFT between n-Decane and DI-water at 300 K for the water/n-decane system

	Interfacial thickness t, Å	Interfacial tension γ, mN/m
Our calculated value	4.5±0.7	65.33±0.12
Experimental Result [31]	4.6±0.2	51.72
MD simulation value [21]	6.5	58.32
MD simulation value [30]	3.90	66±4

Figure 7 shows the salinity effect on both the interfacial thickness and IFT for the salt-water/n-decane interface systems. With an increase in salt concentration from 0 M to 1.0 M, the salt-water/n-decane interfacial thickness has a maximum value when the salt concentration is 0.2 M, as shown in Figure 7(a). Through averaging the IFT fluctuation profile in the period of the last 1 ns with an averaging time step of 10 ps, the corresponding IFT between salt water and n-decane is shown in Figure 7(b). The result indicates an opposite trend in the variation of interfacial thickness with an increase of water salinity. A minimum water/decane IFT value of 61.8 mN/m is predicted at an electrolyte concentration of 0.20 M. The typical calculated DI-water/n-decane interfacial thickness value of 4.5 ± 0.7 Å and IFT of 65.33±0.12 mN/m are obtained, which is

comparable with published experimental and simulation results [21, 30, 31] as presented in Table 2.

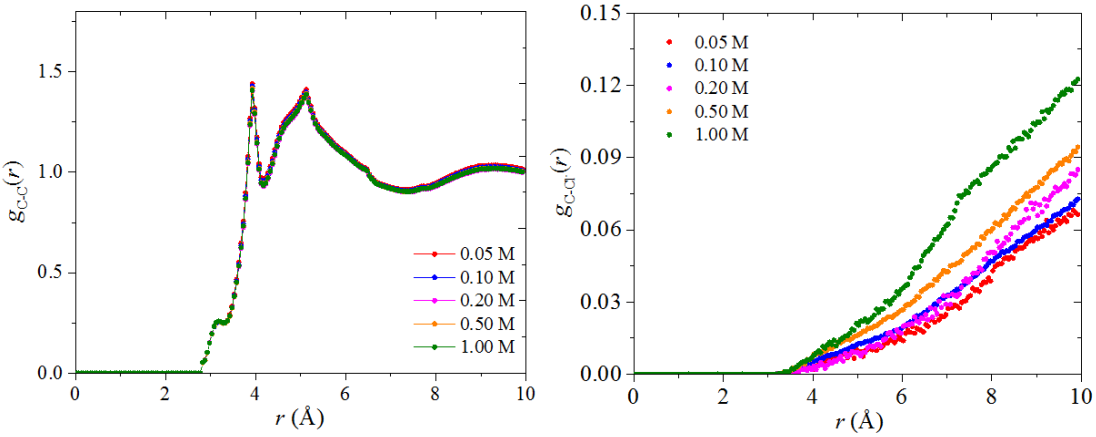

(a) decane carbon – decane carbon (b) decane carbon – chloride ions

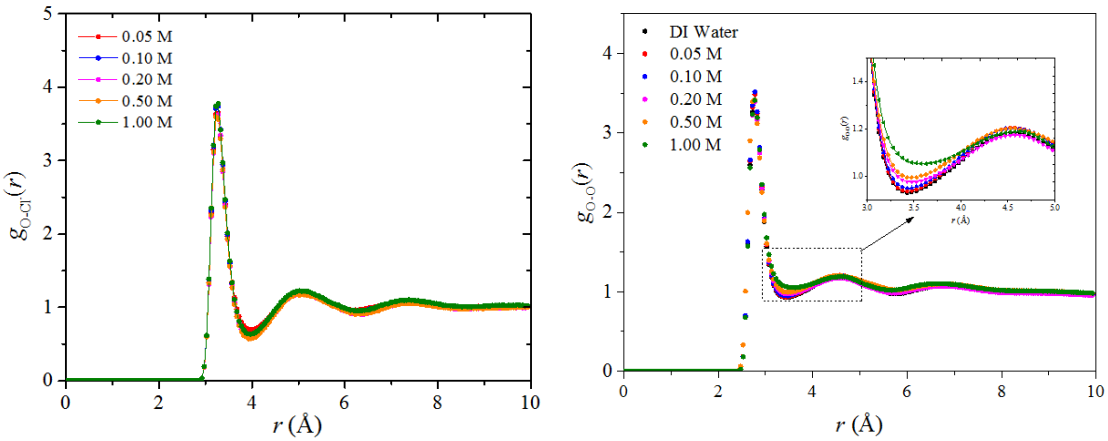

(c) water oxygen- chloride ions (d) water oxygen - water oxygen

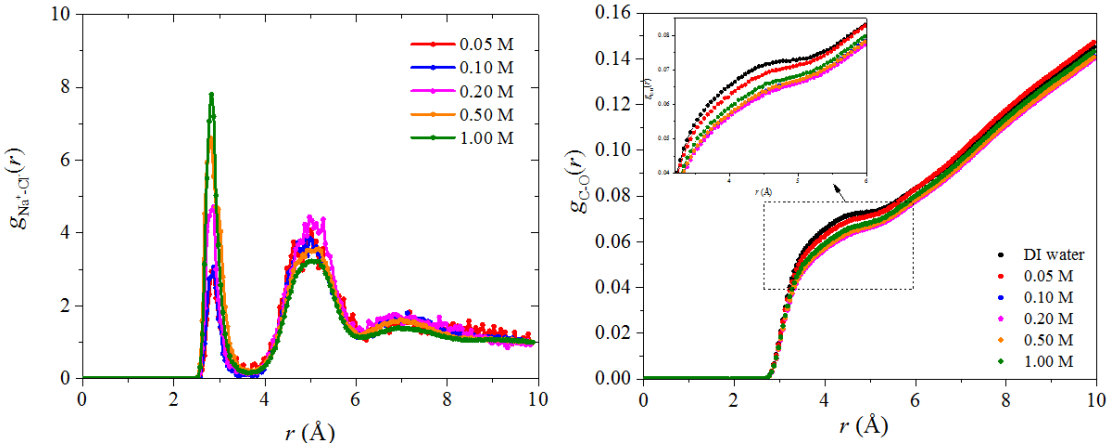

(e) sodium ions - chloride ions (f) water oxygen – decane carbon

Figure 8 The radial distribution functions for salt-water/n-decane interface system

To identify the mechanism by which monovalent ions affect the salt water/oil interface, the radial distribution functions for each component in the salt-water/n-decane binary systems are analysed in Figure 8. It can be observed from the Figure 8(a) that the presence of ions has little effect on the interactions between n-decane molecules in the oil phase. This is due to the insolubility of ions in the decane phase, which is indicated in Figure 8(b) where no dominant peak appeared in the RDF profile, and the ions remain in the water phase. The solubility of the electrolyte ions in the water phase explains the first peak in the RDF profile between ions and water molecules, as shown in Figure 8(c), which represents the hydration structure of the ions. The effect of salinity on the molecular structure of the water phase is displayed in Figure 8(d). It can be seen that the second peak in the water molecule pair correlation function gradually disappears with increasing electrolyte concentration, indicating that the presence of ions forces water molecules to occupy interstitial positions and thus, no well-defined second hydration shell is found around a central water molecule. For the interaction between aqueous Na^+ and Cl^- ions, shown in Figure 8(e), the first peaks at around 3 Å show the presence of contact ion pairs in the solution. The second peak, at around 5.2 Å, corresponds to the presence of solvent separated ion pairs in NaCl solutions. With the increase of electrolyte concentration, the probability of contact ion pair formation increases and that of solvent separated ion pair formation decreases for the solution. The effect of salinity on the interaction between water and the decane phase can be observed from the RDF profile between water and decane molecules, as shown in Figure 8(f). No significant peaks can be observed here, but only a continuously increasing trend, which is consistent with the immiscibility of water and n-decane phases. However, an apparent curvature change is manifested along the increasing RDF profile between 3 and 6 Å, indicating adsorption interactions between water and the n-decane phase at the salt-water/n-decane interface. It can be seen that the weakest adsorption between water and n-decane occurs when the electrolye concentration is 0.20 M, demonstrating the loosest of

the interface structures. This phenomenon also corresponds to the calculated equilibrium "10-50" interfacial thickness variations with water salinity, which is caused by the combination of attractive interactions between the water/ions and repulsive interactions between the n-decane/ions, which controls the IFT between salt water and n-decane phase.

3.3 The effect of the salinity on the n-Decane/water/vapour three phase system

MD simulation results concerning the effect of salinity on the n-decane/water/vapour three phase system are presented in this section. As the initial simulation configurations, outlined in Section 2.1, the rectangular n-decane phase and water slab systems were created with a minimum distance of 4 Å. The final snapshots of an n-decane/water/vapour interface unit cell with different salinities, after 5.0 ns of simulation time, are shown in Figure 9. It can be observed that the n-decane molecules have relaxed to form a 2D cylindrical shape, approaching a lens on the water slab surface caused by attractive interactions due to the van der Waals and Columbic forces between the constituent molecules. After spreading of the n-decane droplet on the water surface it finally forms an elliptically shaped droplet on the water slab surface. After equilibration, the n-decane droplet keeps its shape apart from the effect of thermal fluctuations, as shown in Figure 9.

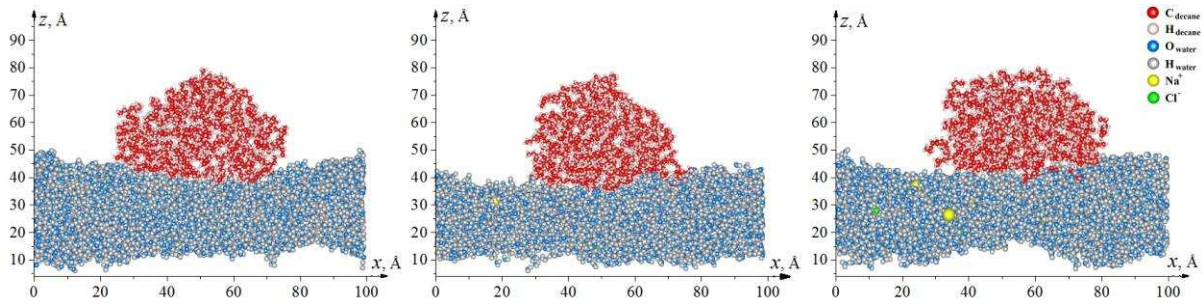

(a) 0 M (b) 0.05 M (c) 0.10 M

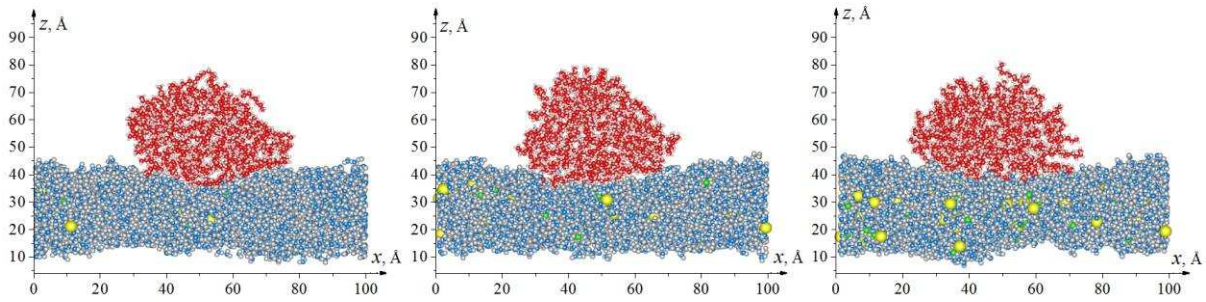

(d) 0.20 M (e) 0.50 M (f) 1.00 M

Figure 9 Series of snapshots of decane-salinity water-vacuum three phase system

During the MD simulation, the three-phase system remains continuous in z-axis direction, as shown in Figure 10. To investigate the detail of the shape of the n-decane/salt-water/vapour three-phase system, the Gibbs dividing surface was calculated from the density profiles of n-decane and water phases along the z-axis direction, as presented in Figure 11. The contact angles were thus obtained from the directions of the upper and lower sides of the n-decane droplet [33], which were fitted as a sphere with a least squares method. To quantify the fluctuation effect in the error analysis, using the block averaging approach, density distributions of each component were calculated over separate 0.2 ns time intervals for the last 2 ns of simulation of the equilibrated trajectory. In this step, a total of 10 density distributions were obtained, resulting in 10 values of contact angle. Further, the equilibrium density distribution and contact angle value were averaged over the last 2 ns. The variance between the averages for these 10 values is presented as the uncertainty. The contact angle variation with water salinity for the three-phase system is presented in Figure 12(a), which indicates a maximum contact angle value of 64.88º at a salinity of 0.20 M. The corresponding interfacial tension variations between salt water and n-decane phases shown in Figure 12(b) have an opposite trend to the contact angle variations. An optimal minimum water/n-decane IFT occurs at a salt concentration of 0.20 M, and such a minimum is considered optimal for enhanced oil

recovery. Qualitatively such a trend is consistent with some experimental studies at the macroscale [40].

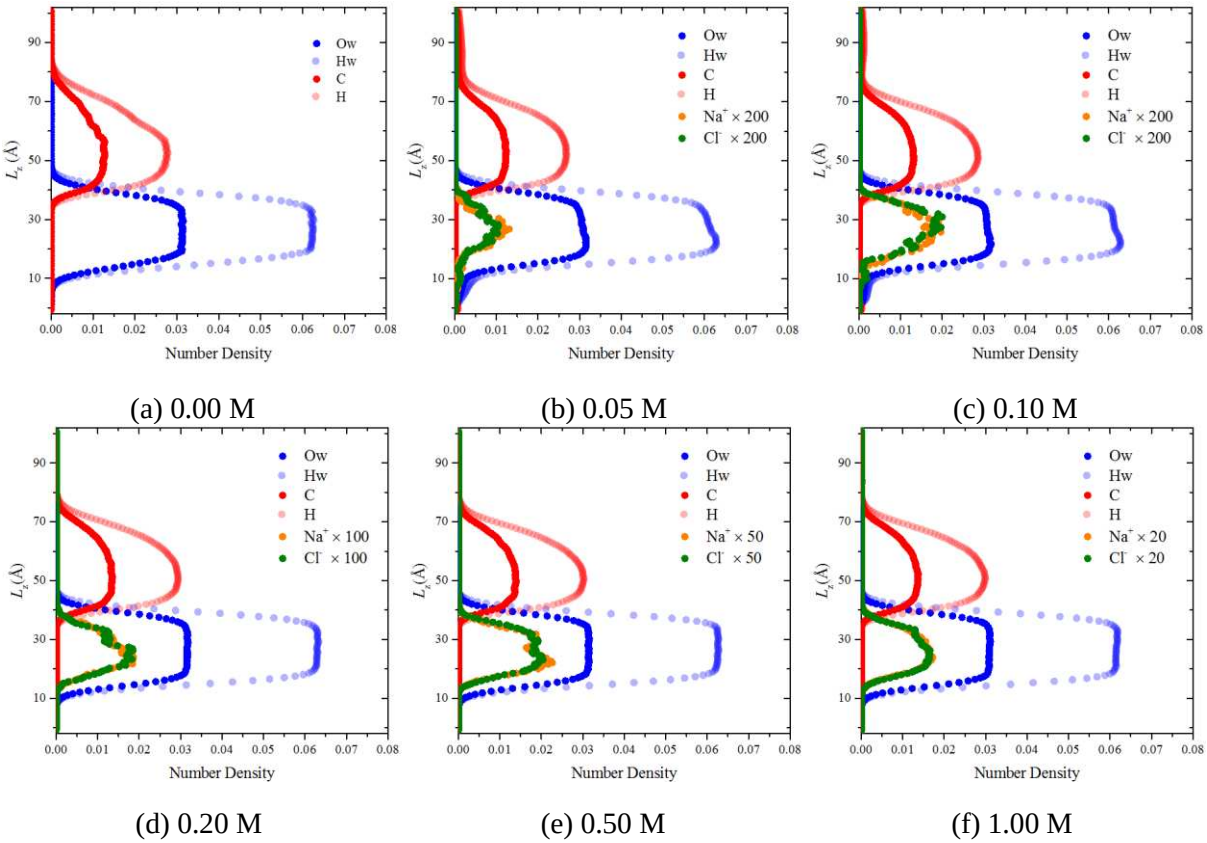

(a) 0.00 M (b) 0.05 M (c) 0.10 M

(d) 0.20 M (e) 0.50 M (f) 1.00 M

Figure 10 Number density along z-axis direction of decane-salinity water-vacuum three phase system

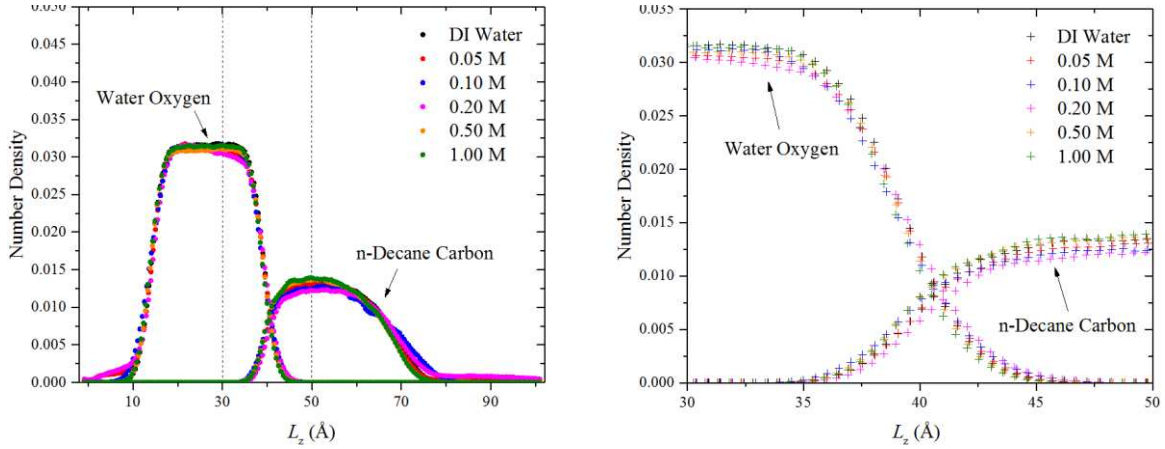

Figure 11 z-density distribution of water oxygen and n-decane carbon at different electrolyte concentrations

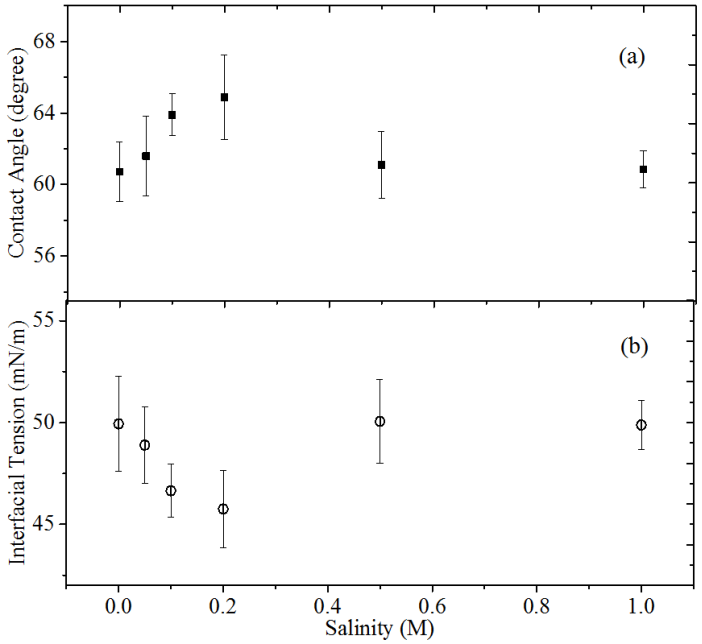

Figure 12 (a) "10-50" interfacial thickness, and (b) surface tension as a function of salinity for n-decane/water/vapour three-phase interface system

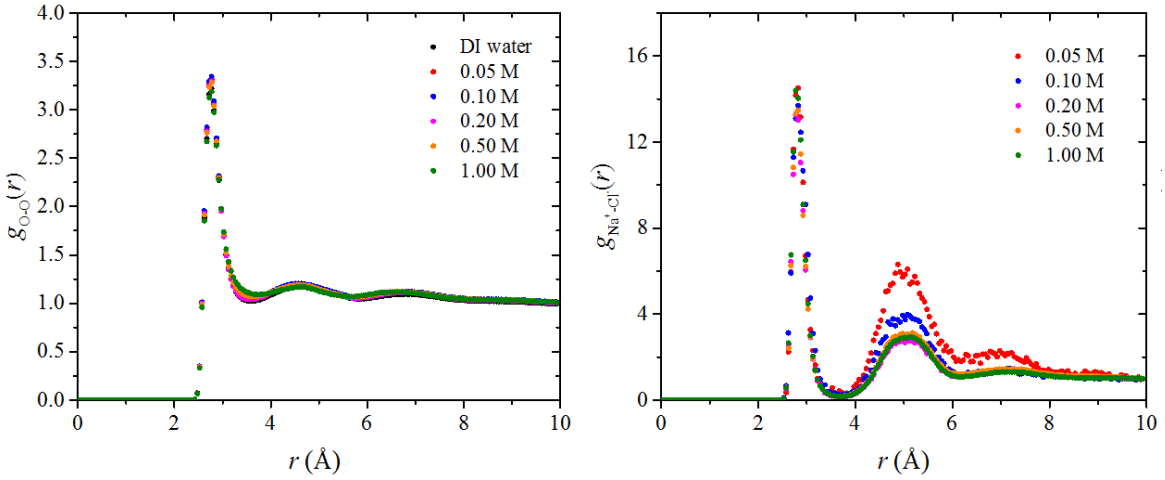

(a) Water oxygen – Water oxygen (b) Sodium ions – Chloride ions

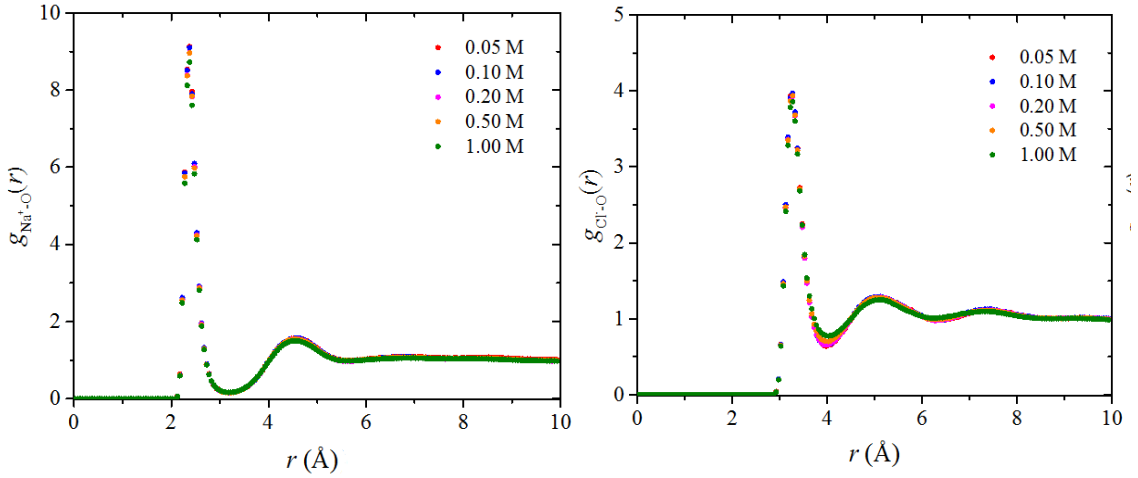

(c) Sodium ions – Water oxygen (d) Chloride ions - Water oxygen

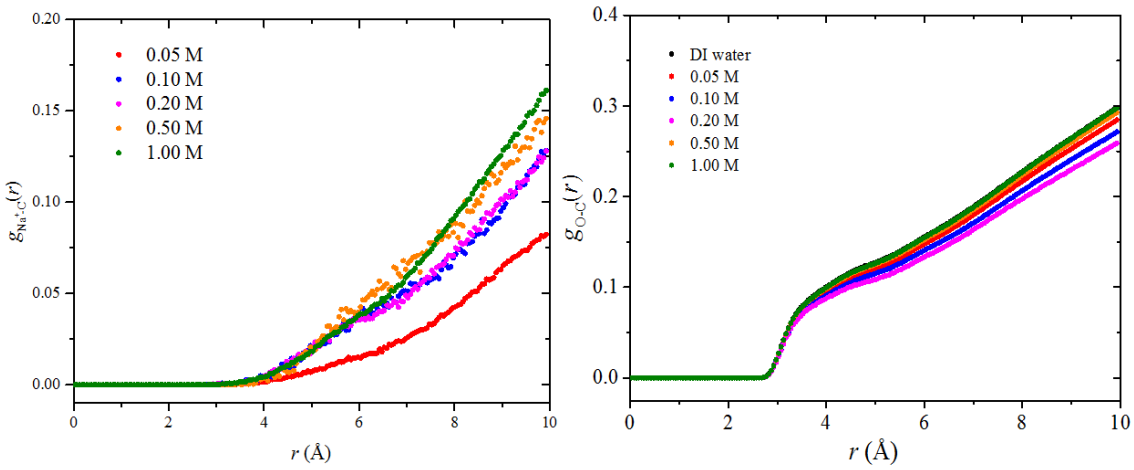

(e) Sodium ions – Decane carbon (f) Water oxygen – Decane carbon

Figure 13 Radial distribution function for water/n-decane/vapour system with different salinity

The radial distribution function profiles for salt-water/n-decane/vapour system are shown in Figure 13. The salinity effects on the water-water, water-ions interaction profiles of salt-water/n-decane/vapour three phase interface system is similar to that for the salt-water/n-decane interface system, as shown in Figure 13(a, b). Both the sodium and chloride ion hydration effect can also be observed as presented in Figure 13(c, d). Figure 13(e) characterises the sodium ion and n-decane molecule interactions as a function of electrolyte concentration. No dominant peaks are observed in the RDF profile between ions and molecules of n-decane in the organic phase, which indicates that all ions remain in the water slab phase instead of transferring to the n-decane phase. Combining the hydration effect of the ions and the repulsion effect between ions and the oil phase, the overall water-oil interaction is shown in Figure 13(f), which suggests that the loosest interface structure between water and n-decane phases is manifested when the electrolyte concentration is around 0.20 M. Qualitatively such trends are consistent with experimental studies at the macroscale [62].

4. Conclusions

As part of increasing our understanding of the mechanism that underpins experimental observations of a benefit in injecting low-salinity water for enhanced oil recovery, otherwise known as 'the salinity effect' molecular dynamics simulation have been performed to model interfaces between water and oil . The results of these simulations can be summarised as follows:

(1) The interfacial tension (IFT) of the water/vapour interface, n-decane/vapour and water/n-decane interfaces were calculated from the pressure tensor distribution after the simulations reached an equilibrated state, with values of 71.43, 20.54 and 65.33 mN/m, respectively. The calculated IFT values show a good agreement with previous experimental and simulation results.

(2) An optimal water salinity value is observed around 0.20 M for the equilibrated water/oil interface system which has the maximum interfacial thickness between water and oil phase, corresponding to the minimum water/oil IFT value.

(3) An optimal water salinity condition at around 0.20 M is also predicted by investigating the equilibrium water/oil/vapour interface system with the maximum contact angle between the water and oil phase, contributing to the minimum salt water/oil IFT value, which is a condition beneficial for enhanced oil recovery.

The presented work indicates that, the molecular level insight into salt-water/oil/vapour interactions and interfacial equilibrium properties offers hitherto un-accessed resolution for EOR applications by using atomistic MD simulation method. Future work shall investigate the salt-water/oil/vapour interactions in a mineral nano slit pore. Both the salinity effect and mineral surface substrate on the oil wettability and recovery factor during EOR shall be modelled.

Acknowledgement

This work was supported by European Research Council Consolidator Grant (Grant Number: 648375) and China Scholarship Council (201506450021).

References

[1] Muggeridge, A.; Cockin, A.; Webb, K.; Frampton, H.; Collins, I.; Moulds, T.; Salino, P.. Recovery rates, enhanced oil recovery and technological limits. Philos. Trans. R. Soc. A. **2014**, 372, 20120320.

[2] Morrow, N.; Buckley, J.. Improved oil recovery by low-salinity water flooding. J. Pet. Technol. **2011**, 63 (05), 106-112.

[3] Jadhunandan, P. P.. Effects of brine composition, crude oil, and aging conditions on wettability and oil recovery. Doc. diss., Dep. Pet. Eng., New Mexico Inst. of Min. Technol. **1990**.

[4] Austad, T.; Shariatpanahi, S. F.; Strand, S.; Black, C. J. J.; Webb, K. J.. Conditions for a low-salinity enhanced oil recovery (EOR) effect in carbonate oil reservoirs. Energy & Fuels. **2011**, 26(1), 569-575.

[5] Sheng, J. J.. Critical review of low-salinity waterflooding. J. Pet. Sci. Eng. **2014**, 120, 216-224.

[6] Nasralla, R. A.; Nasr-El-Din, H. A.. Double-layer expansion: is it a primary mechanism of improved oil recovery by low-salinity waterflooding?. SPE Res. Eval. Eng. **2014**, 17(01), 49-59.

[7] Zhang, H.; Dong, M.; Zhao, S.. Which one is more important in chemical flooding for enhanced court heavy oil recovery, lowering interfacial tension or reducing water mobility?. Energy & Fuels, **2010**, 24(3), 1829-1836.

[8] Underwood, T.; Erastova, V.; Cubillas, P.; Greenwell, H. C.. Molecular dynamic simulations of montmorillonite–organic interactions under varying salinity: an insight into enhanced oil recovery. The J. Phys. Chem. C. **2015**, 119(13), 7282-7294.

[9] Nicolini, J. V.; Ferraz, H. C.; Borges, C. P.. Effect of seawater ionic composition modified by nanofiltration on enhanced oil recovery in Berea sandstone. Fuel, **2017**, 203, 222-232.

[10] Olajire, A. A.. Review of ASP EOR (alkaline surfactant polymer enhanced oil recovery) technology in the petroleum industry: Prospects and challenges. Energy, **2014**, 77, 963-982.

[11] Aveyard, R.; Saleem, S. M.. Interfacial tensions at alkane-aqueous electrolyte interfaces. J. Chem. Soc., Faraday Trans. 1: Phys. Chem. Condens. Phases. **1976**, 72, 1609-1617.

[12] Ikeda, N.; Aratono, M.; Motomura, K.. Thermodynamic study on the adsorption of sodium chloride at the water/hexane interface. J. Colloid Interface Sci. **1992**, 149(1), 208-215.

[13] Badakshan, A.; Bakes, P.. The influence of temperature and surfactant concentration on interfacial tension of saline water and hydrocarbon systems in relation to enhanced oil recovery by chemical flooding, Soc. Pet. Eng. **1990**.

[14] Cai, B. Y.; Yang, J. T.; Guo, T. M... Interfacial tension of hydrocarbon+ water/brine systems under high pressure. J. Chem. Eng. Data. **1996**, 41(3), 493-496.

[15] Serrano-Saldaña, E.; Domínguez-Ortiz, A.; Pérez-Aguilar, H.; Kornhauser-Strauss, I.; Rojas-González, F.. Wettability of solid/brine/n-dodecane systems: experimental study of the effects of ionic strength and surfactant concentration. Colloids Surf. A. **2004**, 241(1-3), 343-349.

[16] Alotaibi, M. B.; Nasr-El-Din, H. A.. Salinity of injection water and its impact on oil recovery. Soc. Pet. Eng. **2009**.

[17] Khusainova, A.; Nielsen, S. M.; Pedersen, H. H.; Woodley, J. M.; Shapiro, A.. Study of wettability of calcite surfaces using oil–brine–enzyme systems for enhanced oil recovery applications. J. Pet. Sci. Eng. **2015**, 127, 53-64.

[18] Fenter, P.; Kerisit, S.; Raiteri, P.; Gale, J. D.. Is the calcite–water interface understood? Direct comparisons of molecular dynamics simulations with specular X-ray reflectivity data. J. Phys. Chem. C. **2013**, 117(10), 5028-5042.

[19] Zhang, H.; Nikolov, A.; Wasan, D.. Enhanced oil recovery (EOR) using nanoparticle dispersions: underlying mechanism and imbibition experiments. Energy & Fuels, **2014**, 28(5), 3002-3009.

[20] Turgman-Cohen, S.; Araque, J. C.; Hoek, E. M.; Escobedo, F. A... Molecular dynamics of equilibrium and pressure-driven transport properties of water through LTA-type zeolites. Langmuir. **2013**, 29(40), 12389-12399.

[21] Berendsen, H. J. C.; Grigera, J. R.; Straatsma, T. P.. The missing term in effective pair potentials. J. Phys. Chem. **1987**, 91(24), 6269-6271.

[22] Jorgensen, W. L.; Tirado-Rives, J.. The OPLS [optimized potentials for liquid simulations] potential functions for proteins, energy minimizations for crystals of cyclic peptides and crambin. J. Am. Chem. Soc. **1988**, 110(6), 1657-1666.

[23] Bankura, A.; Carnevale, V.; Klein, M. L.. Hydration structure of salt solutions from ab initio molecular dynamics. J. Chem. Phys. **2013**, 138(1), 014501.

[24] Jungwirth, P.; Tobias, D. J.. Specific ion effects at the air/water interface. Chem. Rev. **2006**, 106(4), 1259-1281.

[25] D'Auria, R.; Tobias, D. J.. Relation between Surface Tension and Ion Adsorption at the Air− Water Interface: A Molecular Dynamics Simulation Study. J. Phys. Chem. A. **2009**, 113(26), 7286-7293.

[26] Brown, M. A.; D'Auria, R.; Kuo, I. F. W.; Krisch, M. J.; Starr, D. E.; Bluhm, H.; Hemminger, J. C.. Ion spatial distributions at the liquid–vapour interface of aqueous potassium fluoride solutions. Phys. Chem. Chem. Phys. **2008**, 10(32), 4778-4784.

[27] Sun, L.; Li, X.; Hede, T.; Tu, Y.; Leck, C.; Ågren, H.. Molecular dynamics simulations of the surface tension and structure of salt solutions and clusters. J. Phys. Chem. B. **2012**, 116(10), 3198-3204.

[28] Van Buuren, A. R.; Marrink, S. J.; Berendsen, H. J.. A molecular dynamics study of the decane/water interface. J. Phys. Chem. **1993**, 97(36), 9206-9212.

[29] Zeppieri, S.; Rodríguez, J.; López de Ramos, A. L.. Interfacial tension of alkane+ water systems. J. Chem. Eng. Data. **2001**, 46(5), 1086-1088.

[30] Jang, S. S.; Lin, S. T.; Maiti, P. K.; Blanco, M.; Goddard, W. A.; Shuler, P.; Tang, Y.. Molecular dynamics study of a surfactant-mediated decane− water interface: effect of molecular architecture of alkyl benzene sulfonate. J. Phys. Chem. B. **2004**, 108(32), 12130-12140.

[31] Mitrinović, D. M.; Tikhonov, A. M.; Li, M.; Huang, Z.; Schlossman, M. L.. Noncapillary-wave structure at the water-alkane interface. Phys. Review Lett. **2000**, 85(3), 582.

[32] Kunieda, M.; Liang, Y.; Fukunaka, Y.; Matsuoka, T.; Takamura, K.; Loahardjo, N.; Morrow, N. R.. Spreading of Multi-component Oils on Water. Energy & Fuels, **2012**, 26(5), 2736-2741.

[33] Kunieda, M. Molecular Dynamics Study of Oil-Water Interfacial Equilibrium in Petroleum Engineering. PhD Diss., Kyoto Uni. **2012**.

[34] Zhang, C.; Carloni, P.. Salt effects on water/hydrophobic liquid interfaces: a molecular dynamics study. J. Phys. Condens. Matt. **2012**, 24(12), 124109.

[35] Martínez, L.; Andrade, R.; Birgin, E. G.; Martínez, J. M.. PACKMOL: a package for building initial configurations for molecular dynamics simulations. J. Comput. Chem. **2009**, 30(13), 2157-2164.

[36] Dang, L. X.; Smith, D. E.. Molecular dynamics simulations of aqueous ionic clusters using polarizable water. J. Chem. Phys. **1993**, 99(9), 6950-6956.

[37] Underwood, T. R.; Greenwell, H. C.. The Water-Alkane Interface at Various NaCl Salt Concentrations: A Molecular Dynamics Study of the Readily Available Force Fields. Sci. Rep. **2018**, 8(1), 352.

[38] Mohammed, S.; Mansoori, G. A.. Effect of CO2 on the Interfacial and Transport Properties of Water/Binary and Asphaltenic Oils: Insights from Molecular Dynamics. Energy & Fuels, **2018**, 32(4), 5409-5417.

[39] Jian, C.; Liu, Q.; Zeng, H.; & Tang, T.. A Molecular Dynamics Study of the Effect of Asphaltenes on Toluene/Water Interfacial Tension: Surfactant or Solute?. Energy & Fuels, **2018**, 32(3), 3225-3231.

[40] Smith, W.; Yong, C. W.; & Rodger, P. M.. DL_POLY: Application to molecular simulation. Mol. Simul. **2002**, 28(5), 385-471.

[41] Ono, S.; Kondo, S.. Molecular theory of surface tension in liquids. In Structure of Liquids/Struktur der Flüssigkeiten. Springer, Berlin, Heidelberg, **1960;** pp 134-280.

[42] Hill, T. L.. An introduction to statistical thermodynamics. Courier Corporation, **1960**.

[43] Alejandre, J.; Dominic J. T.; Gustavo A. C.. Fluid phase equilibria using molecular dynamics: the surface tension of chlorine and hexane. Mol. Phys. **1995**, 85(3): 651-663.

[44] Senapati, S.; Max L. B.. Computer simulation study of the interface width of the liquid/liquid interface. Phys. Rev. Lett. **2001**, 87(17): 176101.

[45] Ryckaert, J. P.; Bellemans, A.. Molecular dynamics of liquid alkanes. Faraday Discuss. Chem. Soc. **1978**, 66, 95-106.

[46] Spyrou, M.. The Diffusion Coefficient of Water: A Neutron Scattering Study using Molecular Dynamics Simulations. Doc. Diss. Tesis de Maestría, Surrey-Inglaterra, **2009**.

[47] Sorenson, J. M.; Hura, G.; Glaeser, R. M.; Head-Gordon, T.. What can x-ray scattering tell us about the radial distribution functions of water?. J. Chem. Phys. **2000**, 113(20), 9149-9161.

[48] Onsager, L.; Samaras, N. N.. The surface tension of Debye-Hückel electrolytes. J. Chem. Phys. **1934**, 2(8), 528-536.

[49] Flyvbjerg, H.; Henrik G. P.. Error estimates on averages of correlated data. J. Chem. Phys. **1989**, 91.1: 461-466.

[50] Grossfield, A.; Daniel M. Z.. Quantifying uncertainty and sampling quality in biomolecular simulations. Ann. Rep. Comput. Chem. **2009**, 5: 23-48.

[51] Neyt, J.; Wender, A.; Lachet, V.; Ghoufi, A.; Malfreyt, P.. Prediction of the concentration dependence of the surface tension and density of salt solutions: atomistic simulations using drude oscillator polarizable and nonpolarizable models. Phys. Chem. Chem. Phys. **2013**, 15, 11679–11690.

[52] Vega, C.; De, M. E.. Surface tension of the most popular models of water by using the test-area simulation method. J. Chem. Phys. **2007**, 126: 154707.

[53] Chen, Feng; Paul E. S.. Simulated surface tensions of common water models. J. Chem. Phys. **2007**, 126: 221101.

[54] Shi, B.; Shashank S.; Vijay K. D.. Molecular dynamics simulation of the density and surface tension of water by particle-particle particle-mesh method. J. Chem. Phys. **2006**, 124.20: 204715.

[55] Lü, Y. J.; Wei, B.. Second inflection point of water surface tension. Appl. Phys. Lett. **2006**, 89.16: 164106.

[56] Ismail, A. E.; Gary S. G.; Mark J. S.. Capillary waves at the liquid-vapour interface and the surface tension of water. J. Chem. Phys. **2006**, 125.1: 014702.

[57] Alejandre, J.; Dominic J. T.; Gustavo A. C.. Molecular dynamics simulation of the orthobaric densities and surface tension of water. J. Chem. Phys. **1995**, 102.11: 4574-4583.

[58] Jungwirth, P.; and Douglas J. T.. Molecular structure of salt solutions: a new view of the interface with implications for heterogeneous atmospheric chemistry. J. Phys. Chem. B. **2001**, 105.43: 10468-10472.

[59] Bhatt, D.; Chee, R.; Newman, J.; Radke, C. J.. Molecular simulation of the surface tension of simple aqueous electrolytes and the Gibbs adsorption equation. Curr. Opin. Colloid Interface Sci. **2004**, 9(1-2), 145-148.

[60] Wang, X.; Chen, C.; Binder, K.; Kuhn, U.; Pöschl, U.; Su, H.; Cheng, Y. F.. Molecular Dynamics Simulation of the Surface Tension of Aqueous Sodium Chloride: from Dilute to Highly Supersaturated Solutions and Molten Salt. Atoms. Chem. Phys. Discuss. **2017**, 1013.

[61] Cheng, Y.; Su, H.; Koop, T.; Mikhailov, E.; Pöschl, U... Size dependence of phase transitions in aerosol nanoparticles. Nat. Commun. **2015**, 6, 5923.

[62] Al-Khafaji, A.; Neville, A.; Wilson, M.; Wen, D.. Effect of Low Salinity on the Oil Desorption Efficiency from Calcite and Silica Surfaces. Energy & Fuels. **2017**, 31(11), 11892-11901.